JOURNAL OF CATALYSIS 138, 322–342 (1992)

Investigation of Oxidative Coupling of Methane over Bismuth Oxychloride, Samarium Chloride, or Manganese Chloride Supported on Lithium Carbonate–Magnesia Systems

ASHRAF Z. KHAN AND ELI RUCKENSTEIN[1]

Department of Chemical Engineering, State University of New York at Buffalo, Buffalo, New York, 14260

Received March 5, 1992; revised May 14, 1992

The magnesia-supported bismuth oxychloride with lithium carbonate present is significantly more effective and stable with time-on-stream than the unsupported or supported systems free of Li_2CO_3 in the oxidative coupling of methane at 750°C, P_{CH_4} = 20.2 kPa, CH_4/O_2 = 4, and a space velocity of 15,000 $cm^3\ g^{-1}\ h^{-1}$. The most effective catalytic system is obtained when 10 mol% BiOCl is supported on MgO with 10 mol% Li_2CO_3, which leads to a methane conversion of 18%, C_2 selectivity of 83%, and an ethylene-to-ethane molar ratio of 2.9 for at least 12 h under the aforementioned conditions and atmospheric pressure. The unsupported or supported samarium chloride free of Li_2CO_3 was less effective under similar conditions. Only when the samarium chloride and lithium carbonate contents on the support were sufficiently increased (28 and 40 mol%, respectively) the system became effective towards high C_2 selectivity and stability. In contrast, none of the manganese-chloride-based systems exhibited good C_2 selectivity and stability except initially, but they mainly promoted the reaction of methane to carbon oxides. The presence of chlorine, the nature of the cation associated with it and lithium are found to be key factors in determining the performance of the catalysts. The introduction of Li_2CO_3 is found to retard the loss of surface chlorine and prevent the decrease of surface bismuth and samarium, resulting thereby in more stabilized systems. In addition, the bulk and surface modifications, which are more prominent in the presence of Li_2CO_3, caused by calcination and reaction conditions are believed to influence the formation of the catalytically active or inactive sites. The performance of the catalysts is related to its surface composition, bulk modification, decomposition, and reducibility of the metal chlorides or oxychloride on the basis of XPS, XRD, SEM, and thermal analysis (TPD and TPR) investigations.

INTRODUCTION

Many metal oxides, alkali-promoted metal oxides, and mixed metal oxides have been found to be quite effective in the oxidative coupling of methane (OCM) to higher hydrocarbons, principally to ethylene and ethane (*1–31*). It has been reported that the selectivity to ethylene, rather than ethane, can be enhanced when chloride ions are present in the catalyst (*8, 24, 26, 32–39*), or if a chlorine-containing gaseous compound is passed over the catalyst during reaction (*40–44*). From a practical viewpoint the production of ethylene, rather than ethane, is an important consideration in the OCM process.

Burch *et al.* (*42*) observed a high initial ethylene-to-ethane ratio over several chloride catalysts, but in the approach to the steady state this ratio decreased to less than unity. They attributed the initial high ethylene-to-ethane ratio to the gas-phase chlorine radical, the catalysts being the source of these radicals. However, in the course of the reaction that lasted less than 1 h, a substantial loss of chlorine occurred. Thomas *et al.* (*39*) reported that a number of bismuth-oxychloride-containing catalysts exhibited good C_2 selectivity with high ethylene-to-ethane ratios, mentioning some loss in chlorine during reaction. Ahmed and Moffat (*44*), reported that lithium and cesium chlorides supported on silica showed significant improvements in conversion and selectivity

[1] To whom correspondence should be addressed.

0021-9517/92 $5.00

to C_2 hydrocarbons when CCl_4 was continuously added to the gas stream, unlike sodium, potassium, and rubidium chlorides. This indicates that the cationic component of the catalyst also plays a role in the oxidative coupling process. Recently, Lunsford and co-workers (*45*) obtained a stable and active catalyst by incorporating chlorine ions into Li-doped MgO via a sol–gel process but observed that during the 238 h on stream the catalyst lost approximately half of the lithium and chlorine initially present.

Much of the research on chloride-containing catalysts reported thus far has been aimed at attaining high initial conversions and selectivities to C_2 hydrocarbons, with little emphasis on catalyst stability with time-on-stream and its characterization. The purpose of this study is to examine the catalytic stability of BiOCl and to explore the possibility of its increase by employing a substrate (MgO) with or without Li_2CO_3. Almost no information is available on the activity and stability of two other chlorides, namely, $SmCl_3$ and $MnCl_2$, unsupported and supported on MgO with or without Li_2CO_3, although Sm_2O_3 and MnO_2 doped with alkali halides have resulted in effective systems (*11, 42, 46*). We report on the catalytic performance and stability resulting from the addition of different loadings of BiOCl, $SmCl_3$, or $MnCl_2$ to the MgO and Li_2CO_3/MgO systems. The relationship between the catalytic performance and the physico-chemical properties of the catalysts, particularly the extents of surface chlorine, lithium, and cation associated with chlorine, is explored by employing a number of techniques. Preliminary results of our investigations have been presented in Ref. (*47*).

EXPERIMENTAL

Catalyst Preparation

Powdered BiOCl, $SmCl_3 \cdot 6H_2O$, $MnCl_2$, LiCl, MgO, and Li_2CO_3 of 99.9% purity (Aldrich) were used as reagents. The catalysts were prepared by the conventional impregnation method. The procedure comprises the introduction of a known amount of MgO powder into boiling water under vigorous stirring for 30 min, followed by the addition of an appropriate amount of Li_2CO_3, if required. The slurry thus obtained was heated for another 30 min under continuous stirring followed by the addition of an appropriate amount of BiOCl, $SmCl_3 \cdot 6H_2O$, $MnCl_2$, or LiCl. In the case of a transition or alkali metal chloride or oxychloride supported on MgO, the same procedure was followed but without any addition of Li_2CO_3. The resultant suspension was continuously heated with stirring until a thick paste formed. The paste was dried at 120°C overnight in air. The material, white in color, was then compacted at 15,000 psi to form a disk of 20 mm diameter and 3 mm thickness. These disks were broken into small pieces and calcined in air at 750°C for 15 h. After calcination, the white materials became yellowish for BiOCl-containing samples, greyish for $SmCl_3$-containing samples, and black-reddish for $MnCl_2$-containing samples. During calcination some chlorine has evolved out. Some lithium was also lost during calcination. All the calcined materials were ground and sieved to select particle sizes of 80–100 mesh for the catalytic studies.

Catalyst Screening

The methane coupling reactions were performed at 650–800°C under atmospheric pressure by co-feeding the reaction gases (P_{CH_4} = 20.2 kPa, P_{O_2} = 5.05 kPa, P_{He} = 75.9 kPa, and CH_4/O_2 = 4) into a high purity alumina tube reactor (6 mm i.d., 30 cm long) mounted horizontally and heated by a specially constructed (Lindberg 54S-142) single-zone electric furnace (8-cm-long hot zone) with a built-in thermocouple. Usually 200 mg of calcined catalyst sandwiched between quartz wool plugs was placed in the center of the reactor tube, which is connected to the gas inlet and outlet systems through cajon fittings containing high-temperature (250°C) O-ring seals. A stainless steel reactor cap, constructed from a $\frac{1}{4}$″ Swagelok union tee, accommodated an inconel sheathed K-type thermocouple that ex-

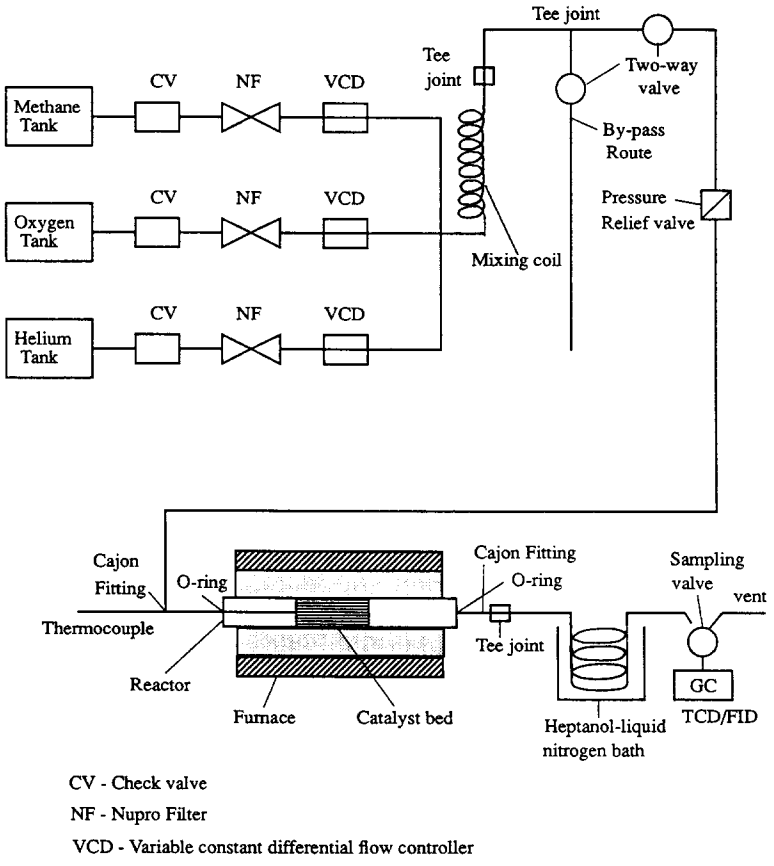

FIG. 1. Schematic diagram of the reactor setup used in the OCM process.

tended into the catalyst bed and measured the temperature with an accuracy of ±3°C. The reactor tube was periodically cleaned with nitric acid to eliminate the carbonaceous and alkali materials deposited on the inside wall. High purity methane, oxygen, and helium (all 99.9% purity; Union Carbide) were used without any additional purification. The flow of each gas was controlled by a variable constant differential flow controller (Porter VCD 1000) which was connected to a Nupro filter (7 μm) and a check valve. The total flow rate measured at the inlet of the reactor was 50 ml/min (NTP). Under the conditions employed, the purely homogeneous gas phase reactions produced less than 1% methane conversion. The schematic diagram of the reactor is presented in Fig. 1.

Product Analysis

The reaction effluents after passing through a heptanol–liquid nitrogen bath (−30°C) were sampled on-line using an automatic 10-port sampling valve and analyzed simultaneously with a dual detector (TCD and FID) GC (PE Sigma 2000) fitted with three different columns and attached to a PE 3600 data station. A Chromosorb 102 column (6 ft × $\frac{1}{8}$ in, 25° isothermal) was used to analyze O_2, CH_4, CO_2, C_2H_4, C_2H_6, and residual H_2O (if any), a molecular sieve 5A column (6 ft × $\frac{1}{8}$ in, 25° isothermal) to separate O_2, N_2, CH_4, and CO, and a Porapak T column (6 ft × $\frac{1}{8}$ in, programmed 25–140°C) to analyze CH_4, C_2H_4, C_2H_6, and C_3 hydrocarbons. The latter product was less than 1 mol% when

explicitly monitored. Nitrogen or argon was used as an internal standard. The response factors for the reactants and products were determined using certified calibration gases (Linde Division). The carbon mass balance was greater than 95% in all experiments.

Catalyst Characterization

The specific surface area of the samples was measured by the BET method with nitrogen adsorption at 77 K. The surface compositions and the valence states of the elements present in the samples were studied by X-ray photoelectron spectroscopy (XPS) using a PHI 500 spectrophotometer. The standard conditions for the analyses were: angle 45°; pass energy 35.75 eV; acquisition time 2–5 min; anode: Mg 300 W. The detail of the procedure can be found in Ref. (*48*). X-ray powder diffraction (XRD) patterns of the catalytic materials were obtained with a Siemens Analytical X-ray Instrument equipped with a curved, position-sensitive detector and a CuK_α source of radiation. The JCPDS files were used to identify the phases (*49*). The morphology and average particle size of selected samples were studied by scanning electron microscopy (SEM, Hitachi S-800). Prior to being studied by SEM, the powdered samples were gold coated in order to eliminate the charging effect. The thermal decomposition and reducibility of the chloride samples were studied by temperature-programmed decomposition (TPD) and temperature-programmed reduction (TPR) techniques according to Refs. (*50, 51*). Hydrogen was the reducing gas, with nitrogen as diluent. The gas flow rates were 0.5 ml/min hydrogen and 5 ml/min nitrogen at NTP. Prior to starting the TPR, each of the samples (50 mg) was heated in flowing nitrogen from 30 to 300°C at a heating rate of 10°C/min and held at 300°C for 1 h. The preheated samples were then subjected to TPR from 300 to 850°C at 10°C/min. A tungsten–rhenium thermal conductivity detector was used for this purpose. For the TPD experiments, H_2 was replaced by N_2 with the conditions and sample amount as above.

TABLE 1

Nominal Composition of the Samples Studied and Their Specific Surface Area

Sample number	Sample designation	Mol% BiOCl[b] ($SmCl_3$, $MnCl_2$, or LiCl)	Mol% Li_2CO_3[b]	Surface area[c] (m^2/g)
1	MgO	0	0	9.8
2	BiOCl[a]	100	0	2.3
3	BiOCl/MgO	10	0	6.7
4	BiOCl/MgO	20	0	n.d.[d]
5	BiOCl/MgO	30	0	n.d.
6	BiOCl/MgO	40	0	4.6
7	Li_2CO_3/MgO	0	10	3.2
8	Li_2CO_3/MgO	0	20	n.d.
9	Li_2CO_3/MgO	0	30	n.d.
10	Li_2CO_3/MgO	0	40	3.0
11	BiOCl–Li_2CO_3/MgO	10	10	2.8
12	BiOCl–Li_2CO_3/MgO	10	20	n.d.
13	BiOCl–Li_2CO_3/MgO	10	30	n.d.
14	BiOCl–Li_2CO_3/MgO	10	40	2.8
15	BiOCl–Li_2CO_3/MgO	40	10	n.d.
16	BiOCl–Li_2CO_3/MgO	40	40	2.9
17	LiCl/MgO	6	0	n.d.
18	LiCl–Li_2CO_3/MgO	7	8	n.d.
19	Sm_2O_3	0	0	4.0
20	$SmCl_3 \cdot 6H_2O$	100	0	2.6
21	$SmCl_3$/MgO	7	0	3.8
22	$SmCl_3$/MgO	28	0	n.d.
23	$SmCl_3$–Li_2CO_3/MgO	7	10	2.8
24	$SmCl_3$–Li_2CO_3/MgO	28	10	2.6
25	$SmCl_3$–Li_2CO_3/MgO	7	40	n.d.
26	$SmCl_3$–Li_2CO_3/MgO	28	40	2.6
27	$MnCl_2$	100	0	3.5
28	$MnCl_2$/MgO	10	0	2.2
29	$MnCl_2$/MgO	40	0	n.d.
30	$MnCl_2$–Li_2CO_3/MgO	10	10	2.2
31	$MnCl_2$–Li_2CO_3/MgO	10	40	n.d.
32	$MnCl_2$–Li_2CO_3/MgO	40	40	2.3

[a] As $BiCl_3$ is converted into BiOCl in the presence of water, the latter was used as catalyst rather than $BiCl_3$.
[b] Values before the preparation of the catalyst.
[c] Measured by the BET method.
[d] n.d. denotes not determined.

RESULTS

Catalytic Performance

Pure magnesium oxide, bismuth oxychloride, samarium chloride, and manganese chloride are low-surface-area (<10 m^2/g) samples (Table 1). For the pure MgO the methane conversion at 750°C is quite low, the main products being ethane and carbon dioxide (Table 2). The ethene-to-ethane molar ratio is as low as 0.2. For the pure BiOCl a similar low activity is observed with a

TABLE 2

Methane Oxidative Coupling Activity over BiOCl-Based Catalysts at 750°C

Sample no.	Catalyst[a]	Conversion (%)[b]		Selectivity (%)				C_2H_4/C_2H_6 Ratio	C_2 yield (%)
		CH_4	O_2	C_2H_4	C_2H_6	CO_2	CO		
1	MgO	4.5	43.2	8.3	39.5	47.5	4.7	0.2	2.1
2	BiOCl	5.0	43.8	15.0	37.0	44.8	3.2	0.4	2.6
3	10% BiOCl/MgO	9.5	79.7	28.2	25.0	44.8	2.0	1.1	5.1
4	20% BiOCl/MgO	10.4	82.1	32.5	26.8	36.2	4.5	1.2	6.2
5	30% BiOCl/MgO	14.7	82.3	36.8	18.0	41.2	4.0	2.0	8.1
6	40% BiOCl/MgO	14.5	81.5	37.5	25.0	31.1	6.4	1.5	8.1
7	10% BiOCl–10% Li_2CO_3/MgO	18.4	62.0	62.0	21.4	16.6	0	2.9	15.3
8	40% BiOCl–10% Li_2CO_3/MgO	22.8	80.5	60.0	16.0	24.0	0	3.8	17.3
9	10% BiOCl–40% Li_2CO_3/MgO	20.7	73.6	58.6	16.3	20.0	5.1	3.6	15.5
10	40% BiOCl–40% Li_2CO_3/MgO	20.2	82.5	56.4	15.6	28.0	0	3.6	14.5
11	10% Li_2CO_3/MgO	9.4	56.9	16.8	21.5	51.1	10.6	0.8	3.6
12	20% Li_2CO_3/MgO	10.5	59.8	18.0	25.7	47.5	8.8	0.7	4.6
13	30% Li_2CO_3/MgO	14.7	51.4	18.1	36.3	37.6	8.0	0.5	8.0
14	40% Li_2CO_3/MgO	12.4	50.5	17.2	53.7	20.3	8.8	0.3	8.8
15	6% LiCl/MgO	11.8	48.2	10.1	30.3	51.4	8.2	0.3	4.8
16	7% LiCl–8% Li_2CO_3/MgO	13.6	52.4	16.1	27.2	48.8	8.0	0.6	5.9

[a] Composition is on mol% basis; space velocity: 15,000 $cm^3\ g^{-1}\ h^{-1}$ (at NTP).
[b] Conversion is in mol%, measured after 1 h of reaction.

slight improvement in the ethene-to-ethane ratio.

When BiOCl was supported on MgO, some increases in the conversion of methane and selectivity to C_2 hydrocarbons were observed. In addition, the ethene-to-ethane ratio became higher than unity. However, upon increasing the BiOCl content from 10 to 40 mol%, no significant change either in the methane conversion or in the selectivity to C_2 hydrocarbons was observed. The ethene-to-ethane molar ratios vary between 1.1 and 2.0.

When 10% Li_2CO_3 was introduced into 10% BiOCl/MgO, the methane conversion increased up to 18 mol% and the selectivity to C_2 hydrocarbons up to 83 mol% compared to 5 and 52%, respectively, for the unsupported BiOCl, the ethene-to-ethane molar ratio being 2.9. Increasing the BiOCl content up to 40 mol% (Li_2CO_3 at 10%) increased the methane conversion to 22.8 mol% and the ethene-to-ethane molar ratio to 3.8, but the C_2 selectivity decreased to 76%. However, for the system with maximum BiOCl and Li_2CO_3 contents (40% BiOCl-40% Li_2CO_3/MgO) there was no significant change in conversion, selectivity, and ethene-to-ethane molar ratio compared to the two systems mentioned above. The C_2 hydrocarbon yield was much higher over the BiOCl–Li_2CO_3/MgO systems than those over unsupported and supported systems free of Li_2CO_3.

Comparison with the Li_2CO_3/MgO systems (without any BiOCl) shows that these catalysts are much inferior to the BiOCl–Li_2CO_3/MgO systems, particularly in terms of C_2 selectivity, yield and ethene-to-ethane ratio. Moreover, increasing the Li_2CO_3 con-

TABLE 3

Methane Oxidative Coupling Activity over $SmCl_3$-Based Catalysts at 750°C

Sample no.	Catalyst[a]	Conversion (%)[b]		Selectivity (%)				C_2H_4/C_2H_6 Ratio	C_2 yield (%)
		CH_4	O_2	C_2H_4	C_2H_6	CO_2	CO		
1	Sm_2O_3	14.0	60.6	13.0	18.8	55.5	12.7	0.70	4.4
2	$SmCl_3$	10.2	63.7	12.3	12.5	70.2	5.0	0.95	2.7
3	7% $SmCl_3$/MgO	14.3	62.7	13.3	12.4	70.2	4.1	1.1	3.7
4	28% $SmCl_3$/MgO	17.3	54.3	18.0	16.8	62.2	3.0	1.1	6.0
5	7% $SmCl_3$–10% Li_2CO_3/MgO	15.1	55.5	23.5	20.0	54.2	2.3	1.2	6.6
6	28% $SmCl_3$–10% Li_2CO_3/MgO	16.3	64.0	35.2	26.3	36.5	2.0	1.3	10.0
7	7% $SmCl_3$–40% Li_2CO_3/MgO	15.5	65.8	36.2	23.5	36.0	4.3	1.5	9.3
8	28% $SmCl_3$–40% Li_2CO_3/MgO	18.4	58.7	57.5	20.0	20.5	2.0	2.8	14.3

[a] Composition is on mol% basis; space velocity: 15,000 $cm^3\ g^{-1}\ h^{-1}$ (at NTP).
[b] Conversion is in mol%, measured after 1 h of reaction.

tent from 10 to 40 mol% decreases the ethene-to-ethane molar ratio from 0.8 to 0.3, although the total C_2 selectivity for 40% Li_2CO_3/MgO is close to that for the BiOCl–Li_2CO_3/MgO systems.

The CH_4 conversions over $SmCl_3$ is higher than that over BiOCl but the C_2 selectivity is much lower (Table 3). However, the C_2H_4/C_2H_6 ratio is somewhat larger for the former. Supporting $SmCl_3$ on MgO does not make any noticeable change in its performance, and increasing its content up to 28 mol% does not bring about any enhancement in conversion and selectivity. Upon introduction of Li_2CO_3 to $SmCl_3$/MgO some increase in the C_2 selectivity and decrease in selectivity to CO_x were observed. However, the C_2H_4/C_2H_6 ratio remained almost unchanged at 1.1–1.2. Only when the $SmCl_3$ content was increased to 28 mol% and that of Li_2CO_3 to 40%, the C_2 selectivity and ethylene-to-ethane molar ratio increased to 77.5% and 2.8, respectively, which are comparable to those observed for 10% BiOCl–10% Li_2CO_3/MgO. The C_2 hydrocarbon yield over this $SmCl_3$-based sample was also comparable to that of the BiOCl-based one.

Unsupported $MnCl_2$ promotes, to a great extent, the formation of carbon oxides, the total C_2 selectivity being less than 20% and the ethylene-to-ethane molar ratio after attaining the steady state being 0.5 (Table 4). It should be mentioned that the initial ethylene-to-ethane ratio over pure $MnCl_2$ was as high as 23.5 but decreased to 0.5 within 20 min of reaction. Unlike BiOCl or $SmCl_3$, supporting $MnCl_2$ on MgO results in an inferior system which drastically reduces the C_2 selectivity and promotes mainly the CO_2 formation. When Li_2CO_3 was introduced into the supported systems ($MnCl_2$/MgO), only a minor increase in methane conversion was observed. Still the carbon oxides remained the major products (higher than 90% selectivity), with C_2 hydrocarbons less than 10% and the ethylene-to-ethane ratio less than 0.7. The C_2 hydrocarbon yield was very low over any $MnCl_2$-based sample.

Figure 2 presents the variation of the total C_2 selectivity with time-on-stream over the catalysts at 750°C. Only two systems, namely, 10% BiOCl–10% Li_2CO_3/MgO and 28% $SmCl_3$–40% Li_2CO_3/MgO, operate in a stable manner for at least 12 h, unlike the

TABLE 4

Methane Oxidative Coupling Activity over $MnCl_2$-Based Catalysts at 750°C

Sample no.	Catalyst[a]	Conversion (%)[b]		Selectivity (%)				C_2H_4/C_2H_6 Ratio	C_2 yield (%)
		CH_4	O_2	C_2H_4	C_2H_6	CO_2	CO		
1	$MnCl_2$	6.2	50.3	6.5	12.5	77.0	4.0	0.5	1.2
2	10% $MnCl_2$/MgO	5.8	75.3	0.1	0.9	93.2	5.8	0.11	0.06
3	40% $MnCl_2$/MgO	10.6	78.2	0.2	1.8	92.0	6.0	0.11	0.2
4	10% $MnCl_2$–10% Li_2CO_3/MgO	13.1	76.1	0.4	1.6	94.4	3.6	0.25	0.3
5	10% $MnCl_2$–40% Li_2CO_3/MgO	12.1	68.7	11.2	17.1	69.6	2.0	0.65	3.4
6	40% $MnCl_2$–10% Li_2CO_3/MgO	16.0	66.4	2.6	4.8	87.6	4.6	0.51	1.2
7	40% $MnCl_2$–40% Li_2CO_3/MgO	15.9	68.0	3.8	5.5	85.7	5.0	0.70	1.5

[a] Composition is on mol% basis; space velocity: 15,000 $cm^3\ g^{-1}\ h^{-1}$ (at NTP).
[b] Conversion is in mol%, measured after 1 h of reaction.

corresponding systems without any Li_2CO_3 and the $MnCl_2$-based systems. The initial high C_2 selectivity with a high ethylene-to-ethane molar ratio (2.9) is maintained, after an initial slight decrease, over the 10% BiOCl–10% Li_2CO_3/MgO system and to a smaller extent over the 28% $SmCl_3$–40% Li_2CO_3/MgO system. The methane conversion did not vary much during this period.

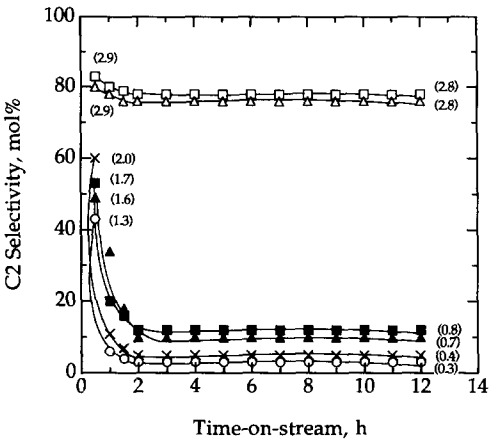

FIG. 2. Change in selectivity to C_2 hydrocarbons with time-on-stream over BiOCl-, $SmCl_3$-, and $MnCl_2$-based catalysts at 750°C. (The numbers in parentheses represent the ethylene-to-ethane ratios.) (■) 10% BiOCl/MgO, (□) 10% BiOCl–10% Li_2CO_3/MgO, (▲) 28% $SmCl_3$/MgO, (△) 28% $SmCl_3$–40% Li_2CO_3/MgO, (○) 40% $MnCl_2$/MgO, (×) 40% $MnCl_2$–40% Li_2CO_3/MgO.

To establish the effect of the contact time on the methane conversion and selectivity, the amount of catalyst was varied while holding the flow rate constant at 50 ml/min. It was found (Fig. 3) that the methane conversion and the selectivity (both to C_2 hydrocarbons and carbon oxides) were dependent on the contact time only for very short contact times (small catalyst content). With the increase in contact time, the conversion and selectivity became more or less independent of the contact time, but the ethylene-to-ethane ratio continued to increase. These observations are consistent with reported values (*52*).

Figure 4 shows that the methane conversion increases with temperature over the three catalysts presented, the BiOCl-based one exhibiting the highest conversion (24%) at 800°C. However, the C_2 selectivity varies differently over these catalysts. Over the BiOCl-based catalyst the C_2 selectivity increases with temperature, that over $SmCl_3$-based catalyst passes through a maximum at

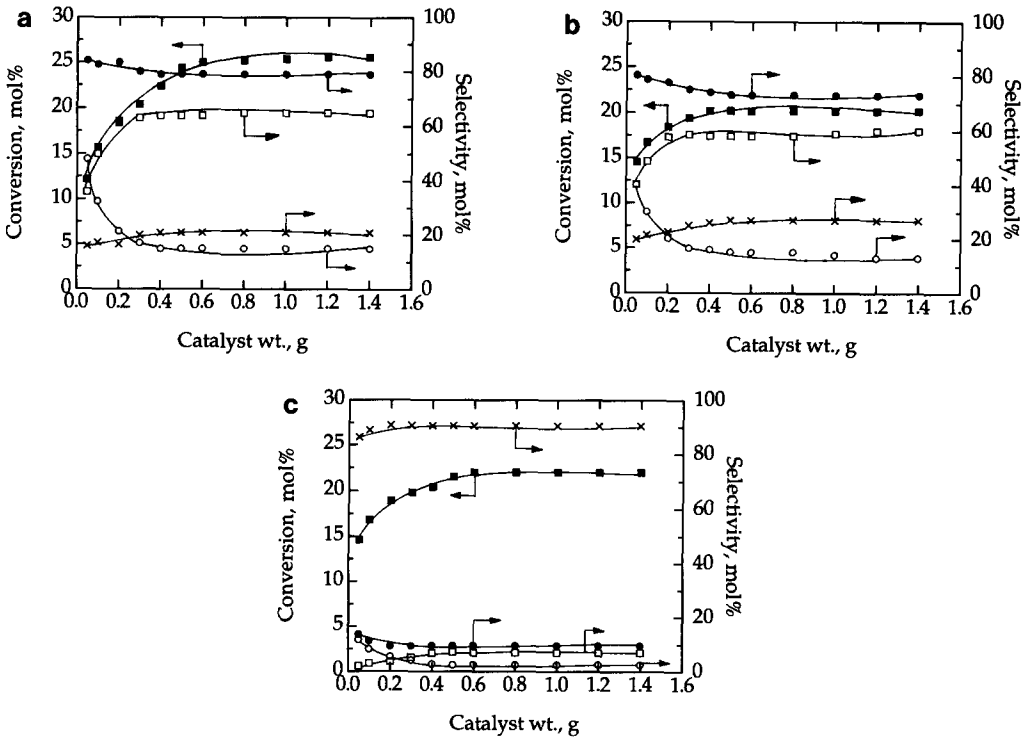

FIG. 3. The effect of contact time on methane conversion (■) and selectivity to C_2H_4 (□), C_2H_6 (○), total C_2 (●), and CO_x (×) over BiOCl-, $SmCl_3$-, and $MnCl_2$-based catalysts at 750°C. (a) 10% BiOCl–10% Li_2CO_3/MgO, (b) 28% $SmCl_3$–40% Li_2CO_3/MgO, and (c) 40% $MnCl_2$–40% Li_2CO_3/MgO.

750°C, whereas that over the $MnCl_2$-based catalyst decreases with increasing temperature. The ethylene-to-ethane molar ratio increases with temperature over the BiOCl- and $SmCl_3$-based samples, but decreases over the $MnCl_2$-based samples.

Figure 5 presents methane conversion and C_2 selectivity as a function of partial pressure of the reactants. The partial pressures of methane and oxygen were changed such that the methane-to-oxygen ratio varied between 2 and 8. It was found that the methane conversion decreased and the C_2 selectivity increased as the methane-to-oxygen ratio increased (higher methane partial pressure). The selectivity to carbon oxides decreased to some extent with the increase in methane-to-oxygen ratio. The three catalysts have similar conversion levels but the BiOCl-based catalyst has a higher C_2 selectivity compared to the $SmCl_3$-based catalyst, whereas the $MnCl_2$-based catalyst showed a negligible C_2 selectivity. The ethylene-to-ethane ratio decreased to some extent with the increase in methane-to-oxygen ratio, except for the $MnCl_2$-based catalyst which showed a negligible C_2 selectivity from the beginning.

XRD Analysis

Pure BiOCl is a crystalline solid. After calcination of BiOCl at 750°C for 15 h a different phase structure emerges which presumably belongs to $Bi_{24}O_{31}Cl_{10}$ (Fig. 6) according to Sillén and Edstrand (*53*). When 10% BiOCl is supported on MgO and calcined at 750°C for 15 h, both MgO and $Bi_{24}O_{31}Cl_{10}$ were detected, with low intensity for the latter and significantly reduced intensity for the former (Fig. 6). Upon intro-

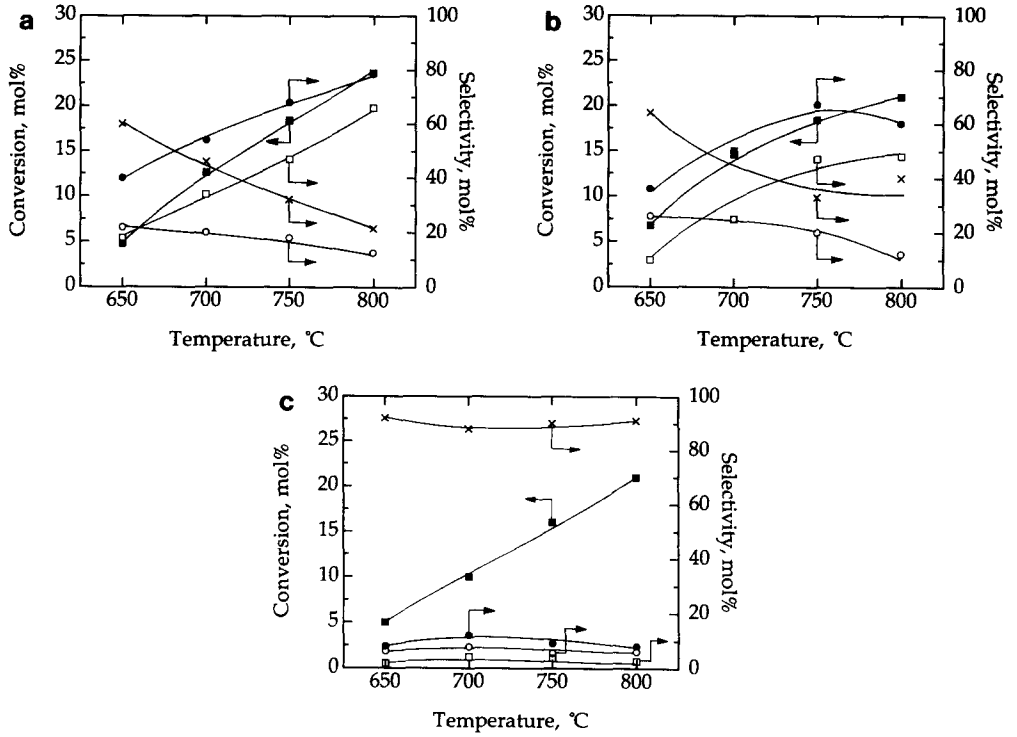

FIG. 4. The effect of reaction temperature on methane conversion (■) and selectivity to C_2H_4 (□), C_2H_6 (○), total C_2 (●) and CO_x (×) over BiOCl-, $SmCl_3$-, and $MnCl_2$-based catalysts at CH_4/O_2 feed ratio of 4. (a) 10% BiOCl–10% Li_2CO_3/MgO, (b) 28% $SmCl_3$–40% Li_2CO_3/MgO, and (c) 40% $MnCl_2$–40% Li_2CO_3/MgO.

ducing 10% Li_2CO_3 to this BiOCl/MgO system, the XRD signals of the calcined samples completely disappeared, indicating that a further structural change has occurred. Increasing the Li_2CO_3 content to 30 or 40 mol%, XRD peaks were again observed for MgO, $Bi_{24}O_{31}Cl_{10}$, and some new compounds such as $LiBi_3O_4Cl_2$. After the catalytic reaction, the 10% BiOCl–10% Li_2CO_3/MgO catalyst exhibited well-resolved XRD peaks which belong to MgO and Bi_2O_3 mainly.

For the calcined $SmCl_3 \cdot 6H_2O$ no new phase (such as Sm_2O_3, SmOCl) was, however, detected, although it has been suggested that SmOCl, whose structure is similar to that of BiOCl, could be obtained in crystallized form under certain conditions (*54, 55*). When 7% $SmCl_3$ is dispersed on MgO support and the sample is calcined at 750°C, the XRD peaks of MgO and $SmCl_3$ become more prominent. Upon introducing 10% Li_2CO_3 to this system and calcining at 750°C for 15 h, mainly MgO, $SmCl_3$, and Sm_2O_3 were detected, whereas after the catalytic reaction only the peaks for MgO and Sm_2O_3 survived. However, when the $SmCl_3$ and Li_2CO_3 contents were increased to 28 and 40%, respectively, on MgO with subsequent calcination, the XRD peaks of MgO, Sm_2O_3, and $SmCl_3$ disappeared, indicating that a largely amorphous solid solution has been formed which escapes detection by XRD. After reaction, this sample shows the presence of the Sm_2O_3 phase mainly.

Pure $MnCl_2$ also shows crystalline behavior but with a smaller peak intensity than $SmCl_3$. Upon dispersing 10% $MnCl_2$ on MgO with subsequent calcination at 750°C for 15 h, the chloride is converted to an ox-

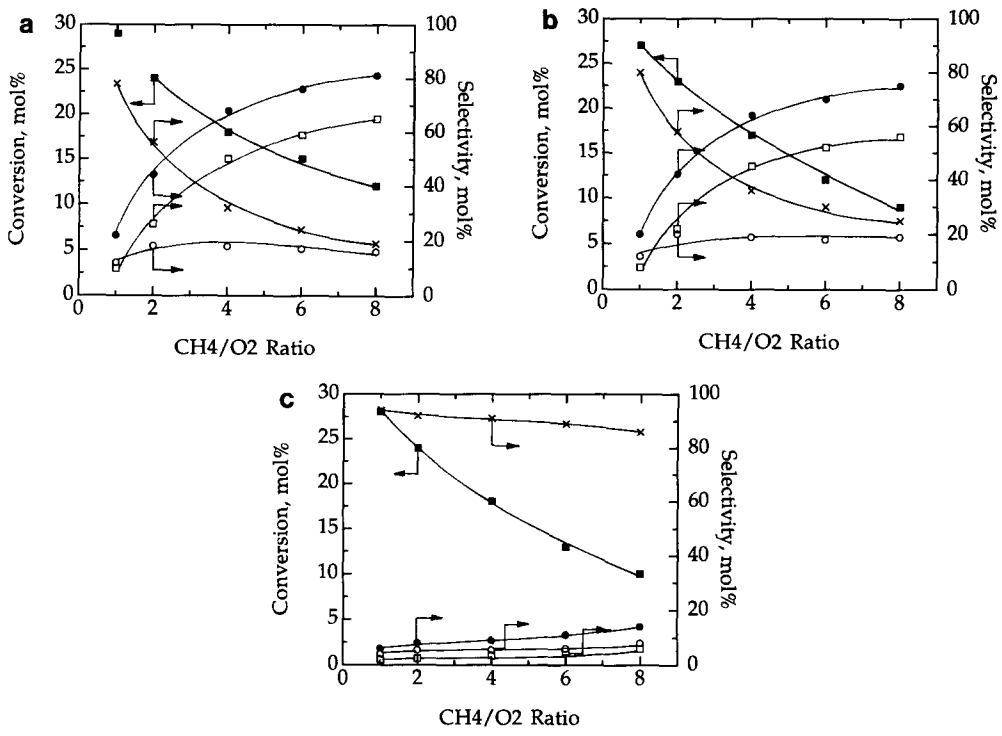

FIG. 5. The effect of partial pressure of the reactants on methane conversion (■) and selectivity to C_2H_4 (□), C_2H_6 (○), total C_2 (●), and CO_x (×) over BiOCl-, $SmCl_3$-, and $MnCl_2$-based catalysts at 750°C. (a) 10% BiOCl–10% Li_2CO_3/MgO, (b) 28% $SmCl_3$–40% Li_2CO_3/MgO, and (c) 40% $MnCl_2$–40% Li_2CO_3/MgO.

ide with a noticeable increase in the peak intensity. Addition of 10% Li_2CO_3 to this system does not result in new peaks, either before or after reaction. However, when the $MnCl_2$ and Li_2CO_3 contents are increased to 40% each and the sample is calcined at 750°C, the peak intensities drastically decrease and after the catalytic reaction they completely disappear (as in the $SmCl_3$-based sample).

Thermal Analyses

Temperature-programmed decomposition (TPD) and temperature-programmed reduction (TPR) studies were performed in order to gain a better understanding of the decomposition and reduction behavior of the calcined catalysts. The analyses were undertaken to identify the temperatures at which intensive dissociation of chlorine from the samples takes place, and also to detect the primary initial species which are present in the catalyst. The reaction conditions used for the TPR experiments are, however, different from those for the methane coupling reactions.

Pure BiOCl dissociates chlorine from its crystalline lattice intensively at 850°C, as can be seen from the TPD profile (Fig. 7). A broken shoulder around 650°C with a smaller intensity indicates that some dissociation takes place at a lower temperature. From 870°C the temperature was kept constant and the change was mainly isothermal. For 10% BiOCl/MgO the dissociation takes place at a lower temperature (780°C) and is almost complete at 870°C, indicating that BiOCl is well dispersed on MgO. For 10% BiOCl–10% Li_2CO_3/MgO the TPD peak reaches a maximum at a much lower temper-

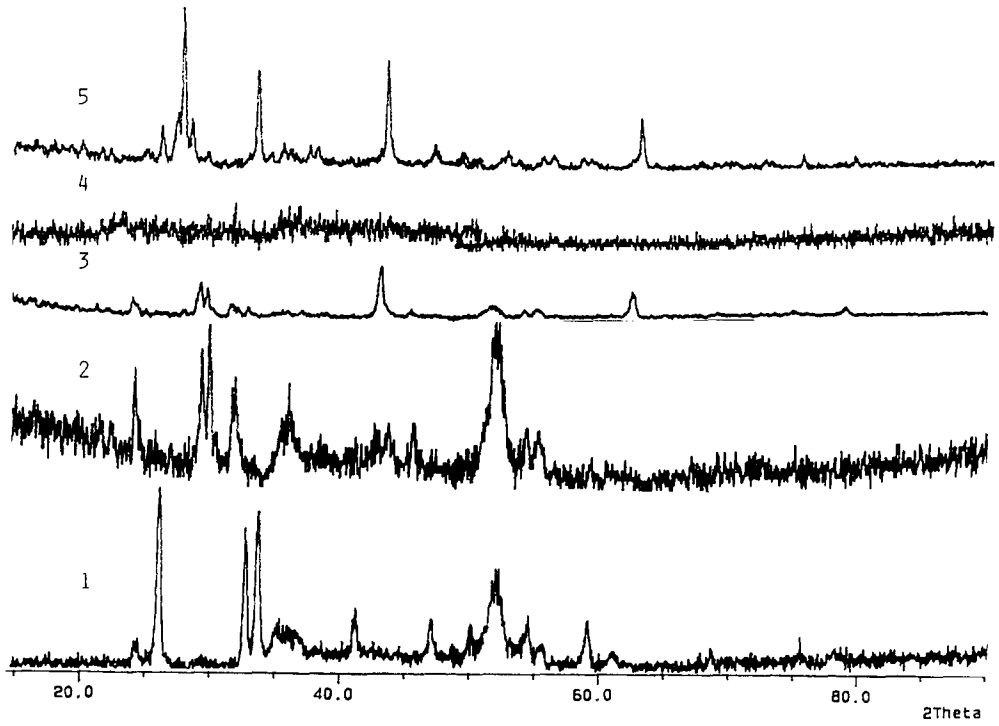

FIG. 6. XRD patterns of the BiOCl-based catalysts after calcination at 750°C for 15 h and after the oxidative coupling of methane at 750°C for 6 h. (For comparison the diffraction pattern for the uncalcined BiOCl is included.) (1) BiOCl (uncalcined), (2) BiOCl (calcined), (3) 10% BiOCl/MgO (calcined), (4) 10% BiOCl–10% Li_2CO_3/MgO (calcined), and (5) 10% BiOCl–10% Li_2CO_3/MgO (post-catalysis).

ature (700°C) and the profile becomes parallel to the baseline from 700 to 870°C and remains parallel during isothermal heating for 2 h at 870°C. This indicates that the decomposition is not complete even under the isothermal condition (870°C). In order to exclude any contribution from CO_2 evolved from Li_2CO_3, the product effluent was passed through a molecular sieve 5A column which traps the CO_2 and moisture. Even then the influence of the underlying decomposition of the Li_2CO_3 cannot be excluded (*56*) since this changes the thermal conductivity of the material.

Pure $SmCl_3$ and $MnCl_2$ release less chlorine than BiOCl under the same conditions as can be seen from the area under the profile, and the peaks for maximum dissociation are at lower temperatures, 680–700°C (Fig. 7). The TPD profiles return to the baseline at 800°C, indicating that the dissociation is presumably complete, unlike BiOCl. For 28% $SmCl_3$–40% Li_2CO_3/MgO no new feature emerges in the TPD profile which shows a broad peak between 625 and 725°C. In contrast, 40% $MnCl_2$–40% Li_2CO_3/MgO exhibits intensive dissociation which reaches a maximum at 750°C and remains parallel to the baseline at that level even under the isothermal decomposition. Evidently, the presence of Li_2CO_3 enhances the decomposition of the compound.

Figure 8 shows the TPR profiles of the various chloride-based samples. In order to exclude any contribution from HCl or other volatile compounds, the products were passed through a liquid nitrogen trap. Pure BiOCl exhibits two peaks, one at 680°C and the other at 800°C, while 10% BiOCl/MgO shows a valley-like TPR profile with the

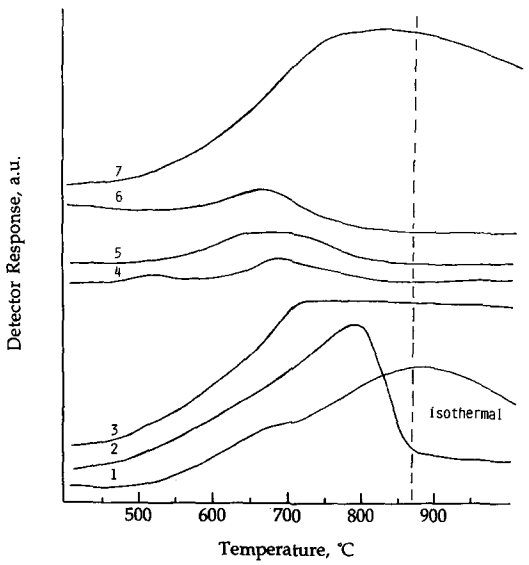

FIG. 7. Temperature-programmed decomposition (TPD) profiles of the BiOCl-, $SmCl_3$-, and $MnCl_2$-based catalysts (50 mg) after calcination at 750°C for 15 h. (From 870°C the decomposition is isothermal, which continues for 2 h.) (1) BiOCl, (2) 10% BiOCl/MgO, (3) 10% BiOCl–10% Li_2CO_3/MgO, (4) $SmCl_3$, (5) 28% $SmCl_3$–40% Li_2CO_3/MgO, (6) $MnCl_2$, and (7) 40% $MnCl_2$–40% Li_2CO_3/MgO.

peaks centered at lower temperatures (620 and 670°C) than before. When doped with Li_2CO_3, the sample shows a narrow peak at 650°C and a broken shoulder at 600°C.

Pure $SmCl_3$ and $MnCl_2$ as well as the MgO-supported chlorides do not show any meaningful TPR profile; only some H_2 uptake is observed. $SmCl_3$ is more inert than $MnCl_2$ under the TPR conditions. Only when 40% Li_2CO_3 is introduced into 40% $MnCl_2$/MgO does the TPR profile show a sharp peak at 725°C.

SEM Studies

The charging effect due to the presence of chlorine has not allowed to obtain very good micrographs. A few for BiOCl are presented in Figs. 9a–9e. The micrograph of the fresh BiOCl clearly shows a randomly distributed layered structure as has been pointed out by Sillén and Edstrand (*53*). After calcination at 750°C for 15 h, the sheets of BiOCl fused together. When 10% BiOCl is supported on MgO and subsequently calcined, the micrographs reveal a granular structure. Addition of the lithium carbonate to the 10% BiOCl/MgO system followed by calcination results in the agglomeration of the granules. After the catalytic experiments at 700–800°C for 6 h, the 10% BiOCl–10% Li_2CO_3/MgO system exhibits again a granular structure with larger and well-shaped granules with small crystallites (presumably $Bi_2O_2^+$) adhered to their surface.

XPS Studies

Table 5 summarizes the electron-binding energies of the Bi 4*f*, Cl 2*p*, Mg 2*p*, Li 1*s*, O 1*s*, and C 1*s* levels detected in the BiOCl-based samples. From the fresh BiOCl to the calcined and post catalysis 10% BiOCl–40% Li_2CO_3/MgO the binding energies for Bi $4f_{7/2}$

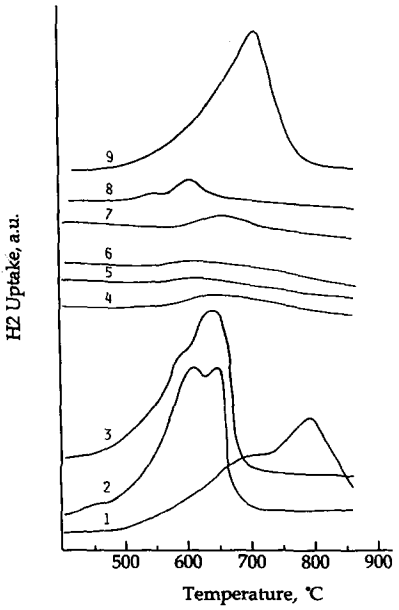

FIG. 8. Temperature-programmed reduction (TPR) profiles of the BiOCl-, $SmCl_3$-, and $MnCl_2$-based catalysts (50 mg) after calcination at 750°C for 15 h. (1) BiOCl, (2) 10% BiOCl/MgO, (3) 10% BiOCl–10% Li_2CO_3/MgO, (4) $SmCl_3$, (5) 28% $SmCl_3$/MgO, (6) 28% $SmCl_3$–40% Li_2CO_3/MgO, (7) $MnCl_2$, (8) 40% $MnCl_2$/MgO, and (9) 40% $MnCl_2$–40% Li_2CO_3/MgO.

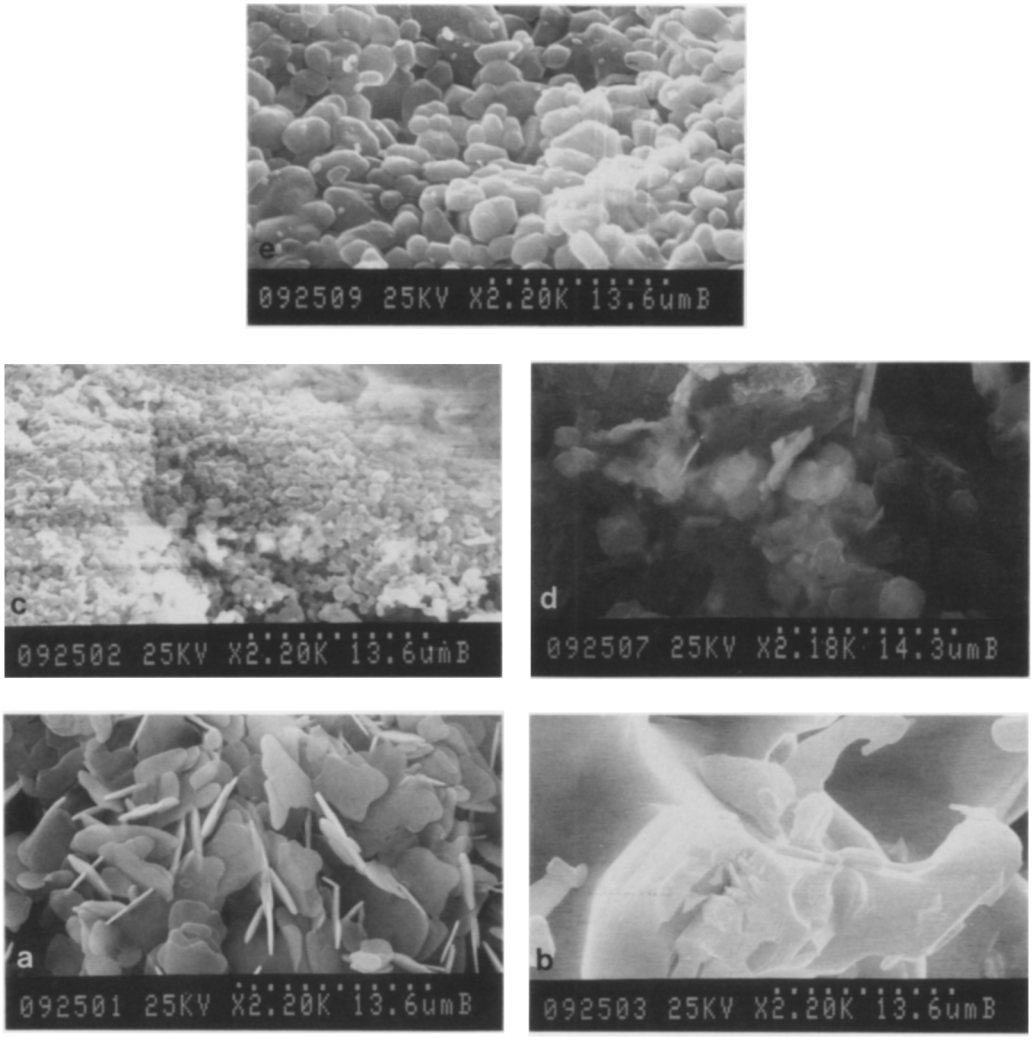

FIG. 9. SEM micrographs of the BiOCl-based catalysts. (a) BiOCl (uncalcined), (b) BiOCl (calcined, 750°C, 15 h), (c) 10% BiOCl/MgO (calcined, 750°C, 15 h), (d) 10% BiOCl–10% Li_2CO_3/MgO (calcined, 750°C, 15 h), and (e) 10% BiOCl–10% Li_2CO_3/MgO (post-catalysis).

are between 158.5 and 159.5 eV, and those for Bi $4f_{5/2}$ between 163.9 and 164.9 eV, which are in agreement with the literature (*48*). These values correspond to trivalent bismuth. The C 1*s* and O 1*s* spectra with binding energies of 285.0–290.4 and 529.2–532.1 eV, respectively, provide evidence that multiple carbon and oxygen species are present on the catalyst surface. The higher binding energy of O 1*s* is ascribed to the carbonate-type, whereas the lower value to the oxide-type oxygen. For C 1*s* the lower binding energy is ascribed to graphite or hydrocarbons and the higher to carbonates (*57*). The Cl 2*p* spectra exhibit a very noisy background due to the charging effect. For some samples, these spectra show a doublet $2p_{3/2}$ and $2p_{1/2}$ with a split of 1.7 eV.

The surface composition of the elements present in the samples after various pretreatments is presented in Table 6. In the fresh BiOCl the surface atomic concentra-

TABLE 5

Electron Binding Energies of the Elements in the BiOCl-Based Samples as Measured by XPS[a]

Sample	Pretreatment or reaction condition	Binding energy (eV)						
		Bi $4f_{7/2}$	Bi $4f_{5/2}$	Mg $2p$	Li $1s$	Cl $2p$	O $1s$	C $1s$
BiOCl	Uncalcined	159.5	164.9	—	—	198.3	530.4	285.0
BiOCl	Calcined, 750°C, 15 h	158.8	164.2	—	—	197.9 199.4	529.9	285.0
BiOCl	Calcined, and reaction with CH_4/O_2, 700–800°C, 6 h	158.8	164.2	—	—	198.0 199.7	529.8	285.0
10% BiOCl/MgO	Calcined, 750°C, 15 h	158.8	164.2	49.2	—	198.4 199.5	530.0 531.9	285.0 290.4
10% BiOCl/MgO	Calcined, and reaction with CH_4/O_2, 700–800°C, 6 h	158.7	164.2	49.5	—	198.9	530.0 532.0	285.0 290.1
20% BiOCl/MgO	Calcined, 750°C, 15 h	158.5	163.9	48.9	—	198.1	529.9 531.8	285.0 289.7
20% BiOCl/MgO	Calcined, and reaction with CH_4/O_2, 700–800°C, 6 h	158.5	163.9	49.3	—	198.3	532.1	285.0 289.9
10% BiOCl–10% Li_2CO_3/MgO	Calcined, 750°C, 15 h	159.0	164.3	49.4	54.9	198.0 199.4	531.7	285.0 290.4
10% BiOCl–10% Li_2CO_3/MgO	Calcined, and reaction with CH_4/O_2, 700–800°C, 6 h	158.9	164.2	49.3	54.9	198.0 199.5	531.7	285.0 290.1
10% BiOCl–40% Li_2CO_3/MgO	Calcined, 750°C, 15 h	159.2	164.6	49.4	—	198.0	531.4	285.0 290.0
10% BiOCl–40% Li_2CO_3/MgO	Calcined, and reaction with CH_4/O_2, 700–800°C, 6 h	158.9	164.4	49.3	—	198.0	529.2	285.0 289.1

[a] For charge referencing the C $1s$ line was used at 285.0 eV.

tions of Bi, O, and Cl are roughly equivalent to the stoichiometric values. After calcination, the Bi content increases to some extent, whereas that of chlorine drastically decreases accompanied by an increase in the oxygen level. After the catalytic reaction the Bi content decreases to some extent, whereas that of chlorine decreases further. These decreases in Bi and Cl contents are more noticeable for the calcined 10 and 20% BiOCl/MgO after the catalytic reactions than those before the reaction. For these supported systems, the C $1s$ spectra reveal the presence of a carbonate species (30%) which is formed due to the adsorption of CO_2 during the reaction and also from the atmosphere by MgO.

The decrease in surface bismuth concentration that occurs during the catalytic reaction is prevented when Li_2CO_3 is added to the BiOCl/MgO but the chlorine concentration decreases further (Table 6). Although the surface chlorine concentrations for the BiOCl–Li_2CO_3/MgO samples show some decrease after the catalytic reaction, these values are still much higher than those for 10 and 20% BiOCl/MgO.

The surface lithium could not be detected in some of the samples investigated (Table 6), which might be related to its high volatility and high ability to diffuse

TABLE 6

Surface Composition of Various Elements in the BiOCl-Based Samples

Sample	Pretreatment or reaction condition	Atomic concentration C_x[a] (%)					
		Bi 4*f*	Mg 2*p*	Li 1*s*	Cl 2*p*	O 1*s*	C 1*s*
BiOCl	Untreated	22.05	—	—	19.23	23.81	34.91
BiOCl	Calcined, 750°C, 15 h	25.67	—	—	6.87	36.63	30.83
BiOCl	Calcined, and reaction with CH_4/O_2, 700–800°C, 6 h	23.79	—	—	5.04	33.95	37.21
10% BiOCl/MgO	Calcined, 750°C, 15 h	2.98	25.67	—	0.74	50.65	19.96
10% BiOCl/MgO	Calcined, and reaction with CH_4/O_2, 700–800°C, 6 h	0.73	23.29	—	0.56	56.75	18.68
20% BiOCl/MgO	Calcined, 750°C, 15 h	3.24	25.00	—	0.73	47.47	23.57
20% BiOCl/MgO	Calcined, and reaction with CH_4/O_2, 700–800°C, 6 h	1.58	22.10	—	0.53	49.25	26.54
10% BiOCl–10% Li_2CO_3/MgO	Calcined, 750°C, 15 h	2.41	4.76	15.98	1.17	53.85	21.83
10% BiOCl–10% Li_2CO_3/MgO	Calcined, and reaction with CH_4/O_2, 700–800°C, 6 h	2.85	18.64	n.d.[b]	1.10	54.60	22.83
10% BiOCl–40% Li_2CO_3/MgO	Calcined, 750°C, 15 h	2.78	17.96	n.d.	4.42	54.47	20.37
10% BiOCl–40% Li_2CO_3/MgO	Calcined, and reaction with CH_4/O_2, 700–800°C, 6 h	3.23	17.25	n.d.	2.26	55.78	21.47

[a] $C_x = (I_x/S_x)/(\Sigma_i I_i/S_i)$, where I = intensity of the peak; S = atomic sensitivity factor.
[b] n.d. denotes not detectable.

into the bulk of the solid (*57*). An appreciable amount of surface lithium far exceeding the bulk stoichiometric value was observed only for the calcined 10% BiOCl–10% Li_2CO_3/MgO system and as a result the surface magnesium concentration became much lower than that in 10% BiOCl/MgO. When lithium could not be detected on the surface, the surface concentration of magnesium increased significantly.

The binding energies for Sm $4d_{5/2}$ were recorded (Table 7) and these values correspond to the trivalent samarium (*48*). As with the BiOCl-based samples, for the $SmCl_3$-based samples the C 1*s* and O 1*s* spectra provided evidence that multiple carbon and oxygen species were present on the catalyst surface. Some platinum impurities (72.0 eV) were found on the surface of 7% $SmCl_3$/MgO. The values for Cl 2*p* levels matched well with those for the BiOCl-based samples. Instead of Mg 2*p*, the spectra for Mg 2*s* levels were recorded whose binding energies corresponded to those in literature (*48*).

The surface chlorine concentration in the MgO-supported $SmCl_3$ samples suffers a drastic decrease during the catalytic reaction and that of samarium also decreases to some extent (Table 8). Although this surface chlorine loss could not be prevented by adding Li_2CO_3 to the system, the samarium content noticeably increased after the catalytic reaction, as also observed with bismuth. The presence of lithium in the surface layer could be detected only for the calcined sample and its value was near to that of the initial bulk value.

TABLE 7

Electron Binding Energies of the Elements in the $SmCl_3$-Based Sample as Measured by XPS[a]

Sample	Pretreatment or reaction condition	Binding energy (eV)					
		Sm $4d_{5/2}$	Cl $2p$	Mg $2s$	Li $1s$	O $1s$	C $1s$
7% $SmCl_3$/MgO	Calcined, 750°C, 15 h	132.8	198.9 199.8	88.5	—	531.8	285.0
7% $SmCl_3$/MgO	Calcined, and reaction with CH_4/O_2, 700–800°C, 6 h	132.8	198.6	88.2	—	532.0	285.0 290.4
28% $SmCl_3$/MgO	Calcined, 750°C, 15 h	132.4	198.6	88.4	—	532.0	285.0 290.4
28% $SmCl_3$/MgO	Calcined, and reaction with CH_4/O_2, 700–800°C, 6 h	132.4	198.6	88.3	—	529.4 532.1	285.0 290.2
28% $SmCl_3$–40% Li_2CO_3/MgO	Calcined, 750°C, 15 h	134.1	198.9 200.3	89.9	56.1	532.3	285.0 290.3
28% $SmCl_3$–40% Li_2CO_3/MgO	Calcined, and reaction with CH_4/O_2, 700–800°C, 6 h	132.0	198.2 199.9	88.4	n.d.[b]	532.0	285.0 289.8

[a] For charge referencing the C $1s$ line was used at 285.0 eV.
[b] n.d. denotes not detectable.

DISCUSSION

Catalytic Performance

The present work demonstrates that the presence of bismuth oxychloride in Li_2CO_3/MgO or of certain compositions of samarium chloride in Li_2CO_3/MgO results in more active and stable catalysts, capable of more selectively converting methane into C_2 hydrocarbons with an appreciable ethylene-to-ethane ratio than the corresponding unsupported or undoped systems. In contrast, manganese chloride, either alone or supported on MgO with or without Li_2CO_3, promotes mainly oxidation to CO_2. This indicates that the nature of the cation associated with chlorine and the presence of Li_2CO_3 are two key factors that determine the selectivity, the ethylene-to-ethane ratio, and the stability of the catalysts. The difference in performance is clearly not a result of surface area. The catalyst that exhibits the best performance in terms of conversion, selectivity, ethylene-to-ethane ratio, and stability (10% BiOCl–10% Li_2CO_3/MgO) has a specific surface area of 2.8 m^2/g, which is comparable to those of the $SmCl_3$- and $MnCl_2$-based samples.

As observed in the present study, the selectivity to C_2 hydrocarbons, particularly that to ethylene, is greatly enhanced in the presence of certain cations (Bi, Sm). Consequently, not only the active chlorine species produced by the interaction of the catalyst with water (which is a by product of OCM) but also the cation plays a role in the enhancement of the coupling process. To verify if, indeed, bismuth plays a role in the process, experiments have been performed by employing LiCl/MgO as well as LiCl–Li_2CO_3/MgO (samples 15 and 16, Table 2). It was found that the C_2 selectivity was much lower than that over the BiOCl-based catalysts with C_2H_4/C_2H_6 becoming less than unity. However, it is not the mere presence of bismuth (or samarium) and chlorine that produces effective and stable catalysts. Only when Li_2CO_3 was added to the BiOCl/MgO, did the system become effective and stable. This suggests that the true active sites for the formation of methyl radi-

TABLE 8

Surface Composition of Various Elements in the $SmCl_3$-Based Samples

Sample	Pretreatment or reaction condition	Atomic concentration C_x[a] (%)					
		Sm $4d_{5/2}$	Cl 2*p*	Mg 2*s*	Li 1*s*	O 1*s*	C 1*s*
7% $SmCl_3$/MgO	Calcined, 750°C, 15 h	4.28	4.07	21.91	—	56.84	12.68
7% $SmCl_3$/MgO	Calcined, and reaction with CH_4/O_2, 700–800°C, 6 h	3.77	1.87	19.05	—	59.33	13.94
28% $SmCl_3$/MgO	Calcined, 750°C, 15 h	12.08	17.58	10.23	—	41.47	18.64
28% $SmCl_3$/MgO	Calcined, and reaction with CH_4/O_2, 700–800°C, 6 h	10.59	8.08	8.90	—	52.43	20.00
28% $SmCl_3$–40% Li_2CO_3/MgO	Calcined, 750°C, 15 h	3.02	30.31	8.86	3.62	31.91	22.28
28% $SmCl_3$–40% Li_2CO_3/MgO	Calcined, and reaction with CH_4/O_2, 700–800°C, 6 h	8.24	4.62	12.91	n.d.[b]	51.92	22.31

[a] $C_x = (I_x/S_x)/(\Sigma_i I_i/S_i)$, where I = intensity of the peak; S = atomic sensitivity factor.
[b] n.d. denotes not detectable.

cals generated, presumably, at the oxychloride/oxide interface are stabilized by the presence of Li.

The effect of operating conditions on the catalysts' performance reported in the present work suggests a possible path to the various reaction products. The generation of methyl radicals by the reactive oxygen species of the catalyst is the primary step in the OCM process (*3*, *4*). These radicals then desorb into the gas phase where they combine to produce ethane, which is partially dehydrogenated to ethylene. Methyl radicals could also react with gaseous dioxygen or oxygen species present on the surface, forming reactive intermediates which decompose to produce carbon oxides. The present findings suggest that the formation of methyl radicals by the catalysts is an important step of the overall synthesis since an empty reactor gave a negligible methane conversion. Presumably, this primary step is facilitated on the catalyst surface, to a greater extent, by the oxygen species than the chlorine species. Indeed, the finding that the CH_4 conversion is changed very little by the presence of chloride catalysts (without Li_2CO_3) indicates that the chlorine species are less likely to enhance the formation of methyl radicals under the conditions employed. The enhancement of ethylene-to-ethane ratio in the presence of certain chloride catalysts suggests that the chlorine species are involved in the generation of C_2H_5 radicals from C_2H_6 and ultimately of C_2H_4 (a sequential product) through a chain reaction (*42*). Since in the absence of the chlorine species the ethylene-to-ethane ratio is very small, the dehydrogenation by the reaction

$$C_2H_6 + 2\,O_s^{2-} \rightleftarrows C_2H_4 + 2\,OH_s^-$$

is not very significant over the chloride catalysts. The methane conversion, C_2 selectivity, and C_2H_4/C_2H_6 ratio are greatly increased when Li_2CO_3 is also present in some of the chloride catalysts. This indicates that the Li_2CO_3 additive plays a major role both in enhancing the generation of active sites for methyl radicals and blocking some of those for carbon oxides.

The increase in ethylene-to-ethane ratio with the contact time observed in 10% BiOCl–10% Li_2CO_3/MgO and 28% $SmCl_3$–40% Li_2CO_3/MgO is also indicative

of sequential reactions in which ethylene is formed via a consecutive reaction pathway involving the dehydrogenation of ethane. The formation of the latter is also facilitated by higher temperature, as evidenced by Fig. 4, suggesting that the gas-phase reactions become important. In addition, the chlorine species, presumably, block to some extent the total oxidation sites on the surface of the catalysts. The moderate decrease in ethylene-to-ethane ratio as the methane partial pressure increases indicates that the dehydrogenation of ethane is retarded by high methane-to-oxygen ratios. This happens because the decreased amount of oxygen shifts the equilibrium between ethane and ethylene in the direction of ethane. The CH_4/O_2 ratio also affects the extent of oxidation of ethane and ethene (*58*).

Relationship between Physico-chemical Properties and Catalytic Behavior

The physical and chemical characteristics of the catalysts, particularly the cooperation among various components, are reflected in their catalytic performance. The XRD analysis reveals that pure as well as BiOCl supported on MgO is transformed into $Bi_{24}O_{31}Cl_{10}$ after calcination and that the system 10% Li_2CO_3–10% BiOCl/MgO fails to present any peaks. After the catalytic reaction, however, the main phases detected were MgO and Bi_2O_3, which indicate that the chloride phase decomposes to a great extent during reaction. Such phase modification does not imply that chlorine is completely lost from the solid. Indeed, the XPS results revealed that the surface chlorine, although in depleted amount, was still present on the solid surface even after the catalytic reaction, and the amount was much higher when Li_2CO_3 was added to BiOCl/MgO, indicating that lithium plays a role in the retention of some of the chlorine. The catalytic stability exhibited by the systems Li_2CO_3–BiOCl/MgO may be related to the stabilization of bismuth on the surface, and to the retention of some chlorine. The fact that lithium disappears from the surface during calcination and reaction is due to its high volatility. Evidently, the introduction of Li is beneficial probably because the vacancies generated by its disappearance from the surface facilitate the formation of active sites.

The TPD experiments show that by supporting BiOCl on MgO, the dissociation temperature is shifted to a lower value (750°C), and to an even lower value (700°C) when Li_2CO_3 is added. For the latter system the decomposition is not complete even during the isothermal heating (870°C), which indicates that the rate of chlorine release is slower than that for BiOCl/MgO. However, the molten state of Li_2CO_3 and the underlying decomposition of the Li_2CO_3 (*56*) phase as well as intraparticle and interparticle mass transfer can affect the TPD peaks.

In an attempt to verify the possible existence of redox sites which are known to facilitate the oxygen transfer between the gas phase and the crystalline lattice, TPR experiments were performed with the calcined samples. Only for the BiOCl-based samples (which are reducible) meaningful TPR profiles were obtained (Fig. 8). The TPR and the XRD analyses are consistent in that while the latter reveals the likelihood of transformation of BiOCl into $Bi_{24}O_{31}Cl_{10}$, and possibly into $LiBi_3O_4Cl$ when Li_2CO_3 is added, the former reveals the existence of two reduction sites which might be related to those complex phases.

The observation that after the catalytic reaction the SEM micrograph of 10% BiOCl–10% Li_2CO_3/MgO sample exhibited a well-shaped granular structure, instead of the initial sheet structure, indicates that the reaction environment facilitates the formation of an active surface layer. The presence of BiOCl disrupts the interactions between Li_2CO_3 and MgO, making the resulting material easy to grind, as also observed during the sample preparation in Ref. (*56*).

The catalysts based on $SmCl_3$ were less active, and only one sample with high $SmCl_3$ and Li_2CO_3 contents (28% $SmCl_3$–40% Li_2CO_3/MgO) resulted in an effective sys-

tem. Although it was suggested that the hydrated precursor $SmCl_3 \cdot 6H_2O$ forms SmOCl upon heating (*55, 59*), no such phase was detected by XRD. Even if a SmOCl phase was formed, it might have escaped XRD detection due to its low concentration. The $SmCl_3$-based samples failed to show any characteristic TPD or TPR profiles, unlike the BiOCl-based samples. The absence of any noticeable TPD peak suggests that the concentration of chlorine released is not high enough under the conditions employed. The relatively inert behavior of the $SmCl_3/MgO$, even after the addition of Li_2CO_3, in the TPR mode indicates that such samples lack any reducible sites, which facilitate the oxygen transfer between the gas phase and the catalyst under the OCM conditions. However, the XPS evidence shows that the addition of lithium carbonate prevents the decrease of the surface samarium concentration in the course of the catalytic reaction, as observed for bismuth. This stabilization of samarium may play a role in the high C_2 selectivity and stability of the catalyst.

Although $MnCl_2$ is likely to form manganese oxychloride under mild conditions (*42*), it is transformed into an oxide under severe conditions. The XRD evidence shows that $MnCl_2$ is transformed into MnO_2 after calcination. The TPR profiles confirm this observation by revealing reduction sites which are characteristics for MnO_2. In view of this transformation into MnO_2, which is well known as a catalyst for complete oxidation of CH_4 to CO_2, it is unlikely that the $MnCl_2$-based samples would produce effective catalytic systems in the OCM process.

CONCLUSION

The following conclusions can be drawn from the present study:

(1) In the OCM process, the formation of ethylene from ethane is a consecutive reaction which is greatly enhanced in the presence of certain oxychloride or chloride catalysts supported on MgO containing Li_2CO_3.

(2) Bismuth oxychloride–lithium carbonate/magnesia as well as some compositions of samarium chloride–lithium carbonate/magnesia act as active, selective, and stable catalysts for the OCM process, yielding up to 15% C_2 hydrocarbons with an appreciable ethylene-to-ethane ratio (2.8–3.8). In contrast, manganese chloride–lithium carbonate/magnesia promotes mainly exhaustive oxidation of methane to carbon oxides.

(3) The nature of the chloride catalyst, reaction temperature, contact time, CH_4/O_2 ratio, and the partial pressures of methane and oxygen are important factors in determining the CH_4 activity, C_2 selectivity, and ethylene-to-ethane ratio.

(4) The performance of the active catalysts is found to depend mainly on the presence of chlorine, the nature of the cation associated with chlorine, and the stabilizing effect of lithium carbonate. In spite of a significant decrease in the surface chlorine during calcination followed by a lower decrease during the catalytic reaction, the BiOCl- and $SmCl_3$-based catalysts remained active, selective, and stable for a period of 12 h.

(5) The precursor materials (BiOCl, $SmCl_3 \cdot 6H_2O$, and $MnCl_2$) are found to exhibit chemical and physical changes under calcination and reaction conditions, and these modifications lead to the formation of active (for BiOCl and $SmCl_3$) or inactive ($MnCl_2$) systems when they are added to Li_2CO_3/MgO.

REFERENCES

1. Keller, G. E., and Bhasin, M. M., *J. Catal.* **73,** 9 (1982).
2. Hinsen, W., Butyn, W., and Baerns, M., *in* "Proceedings, 8th International Congress on Catalysis, Berlin, 1984, Vol. III, p. 581. Dechema, Frankfurt-am-Main, 1984.
3. Ito, T., Wang, Ji-X., Lin, C.-H., and Lunsford, J. H., *J. Am. Chem. Soc.* **107,** 5062 (1985).
4. Driscoll, D. J., and Lunsford, J. H., *J. Phys. Chem.* **89,** 4415 (1985).
5. Ali Emesh, I. T., and Amenomiya, Y., *J. Phys. Chem.* **90,** 4785 (1986).
6. Aika, K.-I., Moriyama, T., Takasaki, M., and Iwa-

matsu, E., *J. Chem. Soc. Chem. Commun.*, 1210 (1986).
7. Otsuka, K., Jinno, K., and Morikawa, A., *J. Catal.* **100,** 353 (1986).
8. Otsuka, K., Liu, Q., and Morikawa, A., *J. Chem. Soc. Chem. Commun.*, 586 (1986).
9. Lin, C.-H., Campbell, K. D., Wang, J.-X., and Lunsford, J. H., *J. Phys. Chem.* **90,** 534 (1986).
10. Imai, H., Tagawa, T., and Kamide, N., *J. Catal.* **106,** 394 (1987).
11. Otsuka, K., and Komatsu, T., *J. Chem. Soc. Chem. Commun.*, 52 (1986).
12. Martin, G. A., Bates, A., Ducarme, V., and Mirodatos, C., *Appl. Catal.* **47,** 287 (1989).
13. Labinger, J. A., Ott, K. C., Mehta, S., Rockstad, H. K., and Zoumalan, S., *J. Chem. Soc. Chem. Commun.*, 543 (1987).
14. Labinger, J. A., and Ott, K. C., *J. Phys. Chem.* **91,** 2682 (1987).
15. Hutchings, G. J., Scurrel, M. S., and Woodhouse, J. R., *J. Chem. Soc. Chem. Commun.*, 1862 (1987).
16. Korf, S. J., Ross, J. A., de Bruijn, N. A., van Ommen, J. G., and Ross, J. R. H., *J. Chem. Soc. Chem. Commun.*, 1433 (1987).
17. Iwamatsu, E., Moriyama, T., Takasaki, N., and Aika, K.-I., *J. Chem. Soc. Chem. Commun.*, 19 (1987).
18. Sofranko, J. A., Leonard, J. J., and Jones, C. A., *J. Catal.* **103,** 302 (1987).
19. Jones, C. A., Leonard, J. J., and Sofranko, J. A., *J. Catal.* **103,** 311 (1987).
20. Hutchings, G. J., Scurrel, M. S., and Woodhouse, J. R., *J. Chem. Soc. Chem. Commun.*, 1388 (1987).
21. Roos, J. A., Bakker, A. G., Bosch, H., van Ommen, J. G., and Roos, J. R. H., *Catal. Today* **1,** 133 (1987).
22. Burch, R., Squire, G. D., and Tsang, S. C., *Appl. Catal.* **43,** 105 (1988).
23. Lee, J. S., and Oyama, S. T., *Catal. Rev.-Sci. Eng.* **30,** 249 (1988).
24. Amenomiya, Y., Birss, V. I., Goledzinowski, M., Galuszka, J., and Sanger, A. R., *Catal. Rev.-Sci. Eng.* **32,** 163 (1990).
25. Larkins, F. P., and Nordin, M. R., *in* "Methane Conversion" (D. M. Bibby, C. D. Chang, R. F. Howe, and S. Yurchak, Eds.), p. 409. Elsevier, Amsterdam, 1988.
26. Cant, N. W., Lukey, C. A., Nelson, P. F., and Tyler, R. J., *J. Chem. Soc. Chem. Commun.*, 766 (1988).
27. Shigapov, A. N., Novozhilova, M. A., Vereshchagin, S. N., Anshits, A. G., and Sokolovskii, V. D., *React. Kinet. Catal. Lett.* **37,** 397 (1988).
28. Lane, G. S. Miro, E. E., and Wolf, E. E., *Appl. Catal.* **53,** 183 (1989).
29. Omata, K., Hashimoto, S., Tominaga, H. and Fujimoto, K., *Appl. Catal.* **52,** L1 (1989).
30. Carreiro, J. A. S. P., and Baerns, M., *J. Catal.* **117,** 258 (1989).
31. Spinicii, R., *Catal. Today* **4,** 311 (1989).
32. Otsuka, K., Liu, Q., Hatano, M., and Marikawa, A., *Chem. Lett.*, 903 (1986).
33. Wohlfahrt, K., Bergfeld, M., and Zengel, H., German Patent 3 503 664 (1986).
34. Otsuka, K., and Komatsu, T., *J. Chem. Soc. Chem. Commun.*, 388 (1987).
35. Fujimoto, K., and Hashimoto, S., Asami, K., and Tominaga, H., *Chem. Lett.*, 2157 (1987).
36. Otsuka, K., Hatano, M., and Komatsu, T., *in* "Methane Conversion" (D. M. Bibby, C. D. Chang, R. F. Howe, and S. Yurchak, Eds.), p. 383. Elsevier, Amsterdam, 1988.
37. Minachev, Kh. M., Usachev, N. Ya., Udut, V. N., and Khodakov, Yu. S., *Russ. Chem. Rev.* **57,** 22 (1988).
38. Baldwin, T. R., Burch, R., Crabb, E. M., Squire, G. D., and Tsang, S. C., *Appl. Catal.* **56,** 219 (1989).
39. Thomas, J. M., Ueda, W., Williams, J., and Harris, D. M., *Faraday Discuss. Chem. Soc.* **87,** 33 (1989).
40. Kimble, J. B., and Kolts, J. H., U. S. Patent 4 620 057 (1986).
41. Withers, H. P., Jones, C. A., Leonard, J. J., and Sofranko, J. A., U.S. Patent 4 634 800 (1987).
42. Burch, R., Squire, G. D., and Tsang, S. C., *Appl. Catal.* **46,** 69 (1989).
43. Burch, R., Crabb, E. M., Squire, G. D., and Tsang, S. C., *Catal. Lett.* **2,** 249 (1989).
44. Ahmed, S., and Moffat, J. B., *Appl. Catal.* **63,** 129 (1990).
45. Hinson, P. G., Clearfield, A., and Lunsford, J. H., *J. Chem. Soc., Chem. Commun.*, 1430 (1991).
46. Otsuka, K., Jinno, K., and Morikawa, A., *J. Catal.* **100,** 353 (1986).
47. Khan, A. Z., and Ruckenstein, E., *Catal. Lett.* **13,** 95 (1992).
48. Wagner, C. D., Riggs, W. M., Davis, L. E., Moulder, J. F., and Muilenberg, G. E. (Eds.), "Handbook of X-ray Photoelectron Spectroscopy," Perking–Elmer Corporation, Minnesota, 1978.
49. J C P D S powder diffraction file, International Centre for Diffraction Data, Swarthmore, 1988.
50. Robertson, S. D., McNicol, B. D., Baas De, J. H., Kloet, S. C., and Jenkins, J. W., *J. Catal.* **37,** 424 (1975).
51. Larkins, F. P., and Khan, A. Z., *Appl. Catal.* **47,** 209 (1989).
52. Chan, T. K., and Smith, K. J., *Appl. Catal.* **60,** 13 (1990).

53. Sillén, L. G., and Edstrand, M., *Z. Kristallogr.* **104,** 178 (1942).
54. Zachariasen, W. H., *Acta Crystallogr.* **2,** 388 (1949).
55. Burch, R., Chalker, S., Loader, P., and Rice, D. A., *Appl. Catal.* **79,** 265 (1991).
56. Larkins, F. P., and Nordin, M. R., *J. Catal.* **130,** 147 (1991).
57. Miro, E., Santamaria, J., and Wolf, E. E., *J. Catal.* **124,** 451 (1990).
58. Burch, R., Chalker, S., Loader, P., Thomas, J. M., and Ueda, W., *Appl. Catal.* **82,** 77 (1992).
59. Cotton, F. A. and Wilkinson, G., "Advances in Inorganic Chemistry," p. 1075. Interscience New York, 1972.